Eidgenössische Technische Hochschule Zürich
Swiss Federal Institute of Technology Zurich

Empa
Materials Science and Technology

Fatigue behavior investigation of additively manufactured Ti-6Al-4V lattices

Research Internship

Daniel Greenfeld

Tuesday 9th July, 2019

Advisors: Dr. Ehsan Hosseini

Empa, Experimental Continuum Mechanics, Prof. Dr. Edoardo Mazza

Acknowledgements

I would like to thank the *Experimental Continuum Mechanics Lab* and Prof. Dr. Edoardo Mazza for the opportunity of doing my research internship there. Special thanks belong to my advisor, Dr. Ehsan Hosseini, who continuously supported and backed the project with great interest and enthusiasm. I would also like to express big thanks to Serjosha Robmann for a fruitful cooperation in the practical parts of the project, as well as for providing the model for the finite element simulation.

I am also thankful for the help that Dr. Holdsworth provided in the analysis of the SEM images.

Finally, I am highly grateful and appreciate the willingness of all colleagues in the lab to help out and answer my project related questions. In this regard, I would like to highlight Dr. Kilian Schillai's and Xiaolong Li's help with the microscope sessions.

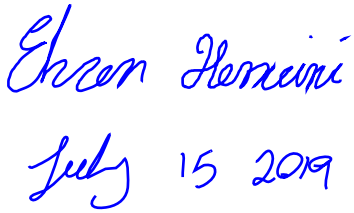

Contents

Contents **iii**

1 Introduction **1**

2 Materials and Methods **3**
2.1 Material 3
2.2 Testing 3
2.2.1 Strut specimens 4
2.2.2 Lattice specimens 5
2.3 Finite element analysis 5
2.4 Microscopic analysis of fracture surfaces 7

3 Results and Discussion **9**
3.1 Fatigue test results of struts 9
3.2 Fatigue test results of lattices 10
3.3 Finite element analysis 10
3.4 Microscopic analysis of fracture surfaces 12
3.4.1 Three different fracture types 12
3.4.2 Co-existence of different fracture types in fatigue specimens 13
3.4.3 Relation of angle of fracture surface and fracture type 13
3.4.4 Analysis of struts 14

4 Summary and Outlook **17**

A Appendix **19**

List of Figures **21**

List of Tables **21**

Bibliography **23**

Chapter 1

Introduction

Conventional manufacturing technologies like machining (milling, turning, drilling, etc.) are subtractive, i.e. material is usually removed from a block of raw material and the final component is built. In additive manufacturing (AM), layer by layer is added to build a component [1]. What is very special about AM is that material synthesis and manufacturing of the component happen simultaneously. This requires a high level of understanding and of control of the process and its parameters to fulfill all quality standards and demands. A big advantage of AM is the high degree of geometrical complexity that can be achieved [1]. One virtually does not have to worry about manufacturability as is the case with conventional manufacturing technologies [1]. Additionally, less material is used and wasted, in contrast to conventional manufacturing technologies where only a small percentage of the raw material results to be in the produced component, while the major amount becomes waste in the form of metallic chips [2]. Even though there are ways to recycle these chips, for some applications and branches, such as the watch industry, it might make sense to switch to AM to increase the efficiency of material use [3]. Experts, however, expect the success of AM to lie in the field of completely new materials with much more complex geometries than used up to now. It is assumed that the manufacturing process with AM is the cheaper the more complex the geometry of the part to be produced is. Moreover, one can build porous structures to achieve a lower weight which is of particular interest for the aerospace industry [4]. In the context of medical technology, implants with enhanced surface properties could be created. In addition, the risk of stress shielding, a well-known problem in load-bearing implants, could be counteracted by producing components that have a stiffness similar to that of bone [5]. More specifically, the stiffness of parts which are critical for the effect of stress shielding, such as the hip implant shaft, could be reduced by using lattice structures. Creating lattice structured parts would also allow for bone ingrowth and could thus

help to achieve a better osseointegration [6]. An exemplary hip implant with lattice structures in its shaft is shown in (Fig. 1.1).

In the biomedical industry, especially in orthopedic technology, Ti alloys belong to the most widely used metals, having high strength to weight and stiffness to weight ratios, corrosion resistance, and compatibility with biomaterials [7]. In fact, the Ti-6Al-4V alloy, which is used in this study, is to date the most widely used titanium alloy by far and corresponds to more than 50% of the annual titanium production [8]. In this project, Ti-6Al-4V samples produced by the selective laser melting (SLM) method were used. SLM is a layer-wise material addition technique which allows production of complex three-dimensional parts by using the thermal energy supplied by a focused and computer-controlled laser beam to selectively melt successive layers of metal powder onto each other [9]. In this research project, it was the goal to investigate the yet not fully understood fatigue behavior of additive manufactured Ti-6Al-4V lattices. In particular, it was the objective to predict the fatigue behavior of lattice structures through the analysis of single struts of the same material.

Figure 1.1: Altair hip implant showing lattice structure in shaft part [10]

Chapter 2

Materials and Methods

2.1 Material

The production of all specimens, both struts and lattices, was realized at Renishaw plc., a British company that offers high-end systems and solutions for metal additive manufacturing. For fabrication of the specimens, an AM250 system, a laser power of 200 W, and Ti-6Al-4V powder were used. Specimens were printed in a vertical direction, i.e. the axis of the building direction was aligned with the long axis of the specimens, and layer thickness was 30 μm. The specimen geometries are depicted in Fig. 2.1. All specimens were annealed at 850° C ±10° C for 2 hours. No surface treatment and no hot isostatic pressing (HIP) treatment were performed. Figures A.1 and A.2 (see Appendix) provide some data about the powder composition of Ti-6Al-4V, as specified by the American Society for Testing and Materials (ASTM), and about the mechanical properties of additively manufactured example components produced by Renishaw, using Ti-6Al-4V powder and a layer thickness of 30 μm.

2.2 Testing

For both strut and lattice specimens, uniaxial fatigue tests were performed in tensile mode. Tensile mode was chosen as tensile loads are known to be more critical than compressive loads for fatigue observations. In fact, compressive loads can slow down crack propagation, as observed in experiments where specimens loaded under fully-reversed regimes have longer fatigue lives than such that are loaded in tension only regimes. All tests were run in force-controlled mode and were performed at room temperature. A stress ratio of $R = 0.1$ was used to avoid compressive loads on and risk of buckling of the specimens, and to allow for comparability with other studies.

An S-N curve and a Haigh diagram were constructed for strut ($n = 10$) and

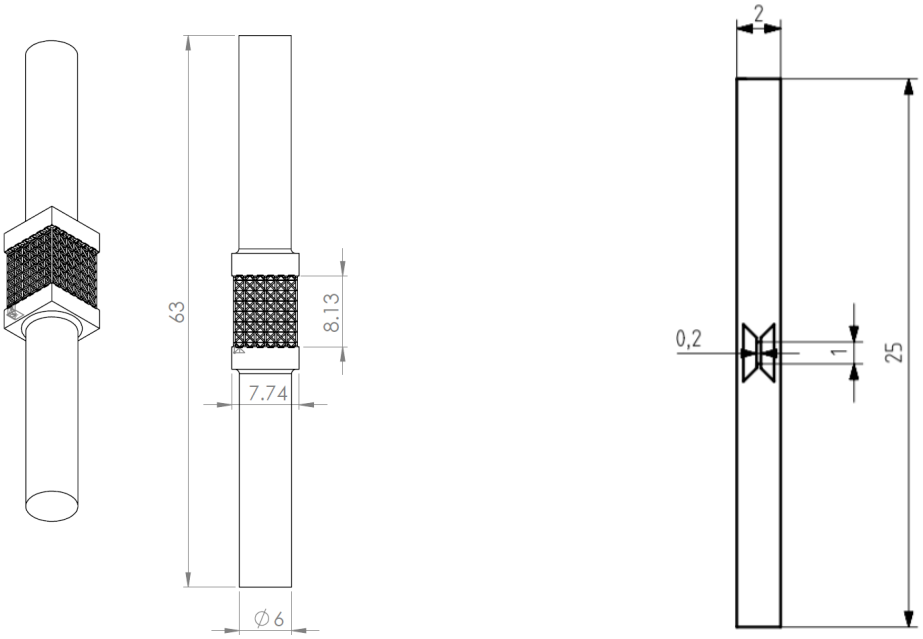

(a) Geometry of lattice specimens

(b) Geometry of struts specimens

Figure 2.1: Geometry of analyzed specimens

Struts	Lattices
149 MPa	386 N
164 MPa	400 N
179 MPa	414 N

Table 2.1: Stress / force levels used for calculation of Median Fatigue Limit for struts and lattices.

lattice ($n = 14$) specimens. In addition, the Median Fatigue Limit (MFL) was determined for a fatigue life of 1 million cycles for both specimen groups using the staircase method according to ISO 12107:2003(E) [11]. Table 2.1 shows what stresses levels were used for the struts and what force levels were used for the lattices to determine the MFL. For the struts, a staircase size of 15 MPa was chosen, while for the lattices it was at 14 N.

2.2.1 Strut specimens

For the strut specimens, a planar biaxial machine with horizontally mounted hydraulic actuators, a hydraulic power unit, and a 100 N load cell (MTS Systems, Eden Prairie, USA) was used to perform the fatigue tests. In a

custom-built test setup, as shown in (Fig. 2.2), the specimens were clamped at 9 mm from the distal end of the specimen between axes 1 and 3 of the machine. Axis 3 was used as the actuated one, while axis 1 was kept static.

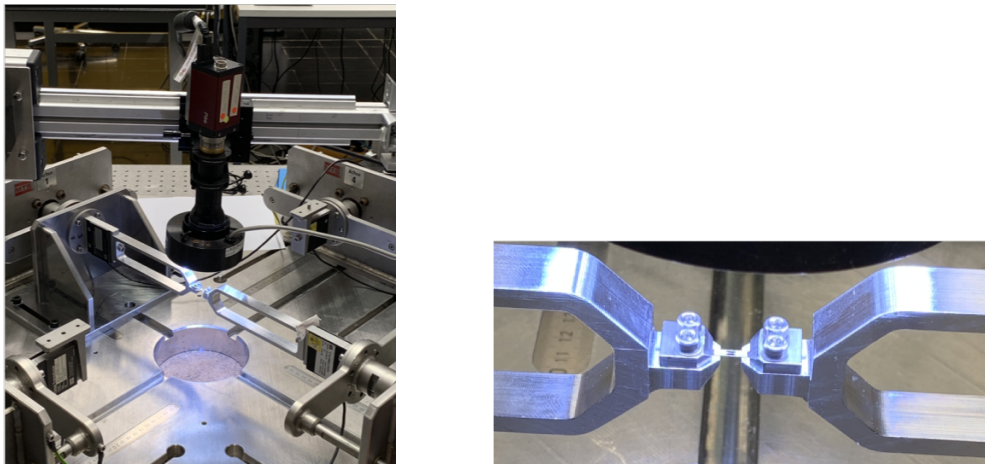

(a) Test setup for struts

(b) Close up of clamped test specimen

Figure 2.2: Test setup for fatigue behavior investigation of struts

2.2.2 Lattice specimens

For the lattice specimens, a servohydraulic test system with a 100 kN load cell (MTS Systems, Eden Prairie, USA) was used to perform the fatigue tests. Figure 2.3 shows the setup of the test. The specimens were clamped at 20 mm from the distal end.

2.3 Finite element analysis

Determination of the cross-sectional area in the lattices to calculate the stresses applied is not trivial. Thus, two different approaches were employed. One very simplified approach was to take the cross-sectional area of the 49 vertical struts ($7x7$ struts) with a strut diameter of 0.2 mm (as specified in the CAD file). In this simplified approach, however, neither the geometrical mismatch that is due to the limited resolution of the manufacturing process, nor the presence of diagonal struts was considered. For this reason and as an alternative to the simple approach, a finite element model of the whole lattice was used to calculate the effective cross-sectional area under load. A 3D surface model was created from 2D computer tomography images of one of the lattices using *Materialise Mimics* software. A Chaboche-type elasto-plastic material model with two back stress components and a displacement boundary condition was used. More specifically, 0.02 mm displacement was

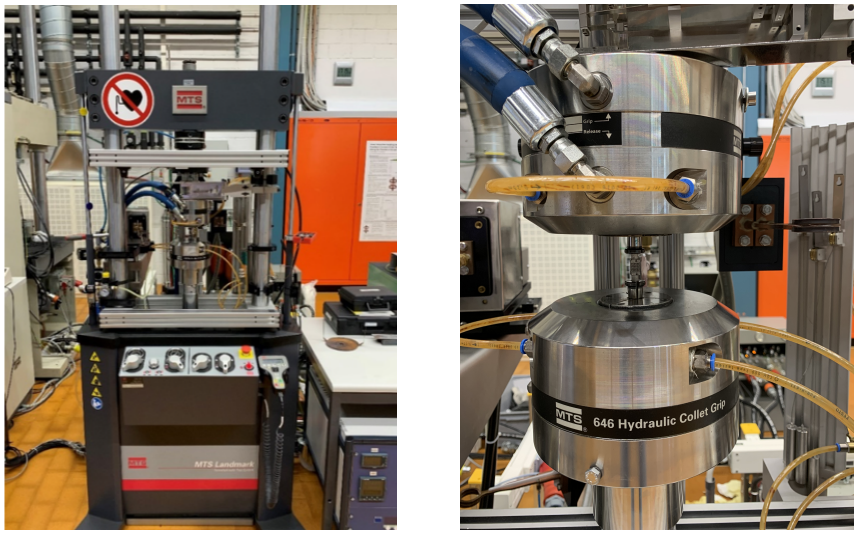

(a) Test setup for lattices (b) Close up of clamped test specimen

Figure 2.3: Test setup for fatigue behavior investigation of lattices

applied to the specimen in z-direction (long axis of the lattice specimen). The material parameters as well as information about the element type and mesh size are provided in table 2.2.

Material parameters and element information
E-Modulus = 105 GPa
Poisson's ratio = 0.34
Elasticity limit = 600 MPa
Strain hardening coefficients: 200, 40 GPa
Strain softening coefficients: 1333, 160
Element type: tetrahedral, C3D10
Adaptive mesh size: = $0.05 - 0.5$ from surface to body

Table 2.2: Material parameters, element type and mesh size used for simulation of the FE model

Rewriting Hooke's law, one can find a formulation to calculate the effective cross-sectional area of a loaded specimen, given force, E-modulus and elastic strain values. For the determination of the E-Modulus, a set of specimens was screened in computer tomography and experimentally tested in quasi-static tests. Then a 3D model of the specimens was used in finite element analysis and in an optimization code that aimed at determining the material parameters in a way that the FE results could best match with the experimental results of the same specimens. I will, however, not further elaborate on

this process as this belongs to a different project. For the force, the reaction force that resulted from applying 0.02 mm displacement to the specimen was taken. Finally, elastic strain was calculated using two points on the long axis of the specimen, measuring their distance before and after applying the displacement to the specimen.

$$A = \frac{F}{E * \varepsilon_{el}} \tag{2.1}$$

2.4 Microscopic analysis of fracture surfaces

The fracture surface of the tested specimens was analyzed under the light microscope and under the scanning electron microscope (SEM) and compared with specimens tested in quasi-static mode. For the fatigue specimens, a fatigue type fracture with striations was expected, while for the quasi-static specimens ductile fractures were predicted. For the SEM analysis, a detector of Everhart-Thornley type and a voltage of 20 kV were used. Pictures were taken with different magnifications, as seen in the *Results and Discussion* section.

Chapter 3

Results and Discussion

3.1 Fatigue test results of struts

Figure 3.1 shows the S-N curve and the Haigh diagram for the struts. The MFL was determined to be at 166.5 $\pm$ 6.1 MPa and is displayed with a red asterisk in the S-N curve. The Haigh diagram should indicate which combinations of stress amplitudes and mean stresses are safe for the given material. Due to the limited amount of data, however, I recommend that the data be treated with caution. Ideally, additional tests at different R-ratios should be conducted and their results should be considered for construction of the Haigh diagram. The staircase test data are found in Table 3.1.

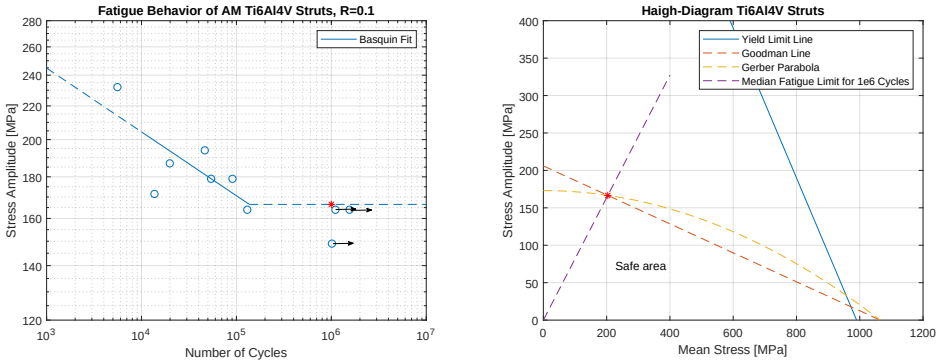

(a) S-N curve for AM Ti6Al4V struts. (b) Haigh diagram for AM Ti6Al4V struts.

Figure 3.1: Fatigue behavior of AM Ti-6Al-4V struts.

Stress level i	Stress amplitude [MPa]	Result					
1	179		X		X		
0	164	O		O		X	
	149						O

Table 3.1: Results of tests used for calculation of Median Fatigue Limit for struts. X = failure, O = run-out

3.2 Fatigue test results of lattices

Figure 3.2 shows the F-N curve for the lattices and a fatigue ratio plot. The fatigue ratio is defined as

$$Fatigue\,Ratio = \frac{Fatigue\,Strength}{Ultimate\,Tensile\,Strength} \tag{3.1}$$

and is frequently used to compare different materials. The MFL for the lattices was determined to be at 397.7 $\pm$ 5.7 N and is displayed with a red asterisk in the corresponding F-N curve. The staircase test data are found in Table 3.2.

Force level i	Force amplitude [N]	Result					
2	414					X	
1	400		X		O		X
0	386	O		O			

Table 3.2: Results of tests used for calculation of Median Fatigue Limit for lattices. X = failure, O = run-out

The fatigue ratio plot shows that both struts and lattices perform worse than bulk AM Ti6Al4V and than wrought Ti6Al4V. Moreover, one can see that lattices perform worse than struts. The reason for the latter observation might be that the lattices contain many more struts and thus the probability for each lattice to have a weak strut that could act as a starting point for development of fatigue cracks is higher than for a single strut to be weak. Additionally, stress concentration in the lattice structures is assumed to be higher than in the struts which could also have a major impact on how lattices perform versus struts.

3.3 Finite element analysis

Finite element analysis helped to determine the effective area under load in the lattice specimens. The resulting S-N curve for the lattices was found to be far more realistic - showing lower fatigue strength values - than the

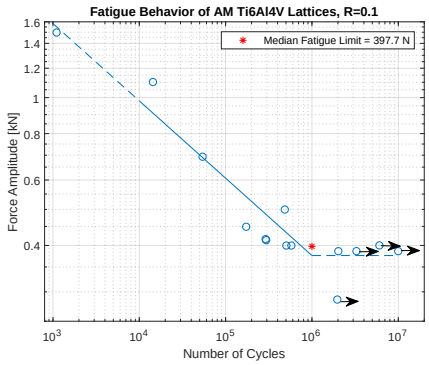

(a) F-N curve for AM Ti6Al4V lattices.

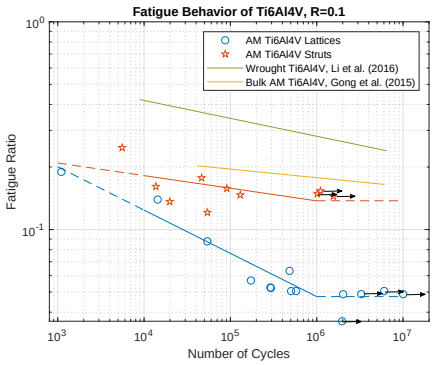

(b) Fatigue ratio plot for AM Ti6Al4V struts and lattices, and bulk AM Ti6Al4V as well as wrought Ti6Al4V.

Figure 3.2: (a) Fatigue behavior of AM Ti-6Al-4V lattices and (b) fatigue ratio plot comparing struts and lattices with bulk AM Ti6Al4V and wrought Ti6Al4V.

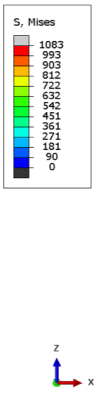

(a) FE model of lattice specimen.

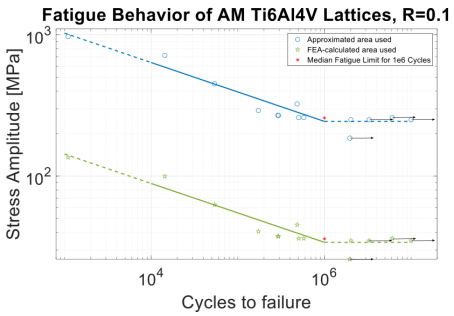

(b) S-N curves for lattices. Blue: Stresses calculated using approximated area. Green: Stresses calculated using area from FE simulation.

Figure 3.3: Fatigue behavior of lattices.

one where the area of 49 vertical struts with an idealized diameter was used. Not only were the diagonal struts considered, but also it proved to be true that due to the geometrical mismatch that led to much thicker struts and to mass accumulation at the nodes the area under load should increase and thus the stresses should decrease.

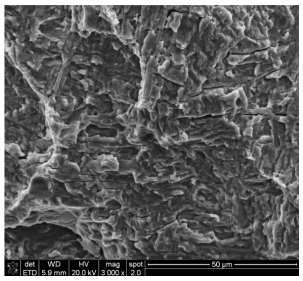

(a) Brittle intergranular fracture surface.

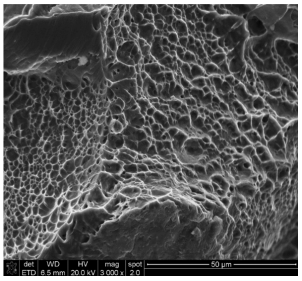

(b) Ductile transgranular fracture surface.

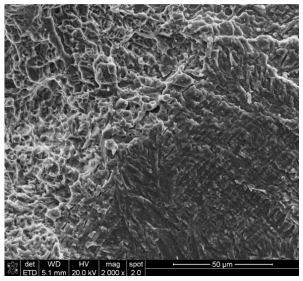

(c) Fracture surface with both ductile transgranular as well as brittle intergranular areas.

Figure 3.4: The three different fracture types observed: (a) Brittle intergranular (b) Ductile transgranular (c) Mixed fracture surface

3.4 Microscopic analysis of fracture surfaces

In the SEM analysis, three main observations were made:

1. Three different fracture types observed overall
2. Co-existence of different fracture types in fatigue specimens
3. Relation of angle of fracture surface and fracture mechanism:
    - for tensile specimens: always ductile transgranular fracture mechanism (both in quasi-perpendicular and in 45° planes) $\rightarrow$ shear stress dominant
    - for low-cycle fatigue (LCF) specimens: ductile transgranular fracture in 45° planes and brittle intergranular fracture in quasi-perpendicular planes
    - for high-cycle fatigue (HCF) specimens: brittle intergranular fracture mechanism observed at most surfaces

3.4.1 Three different fracture types

Figure 3.4 shows three SEM pictures that represent the three different fracture types that were observed. More specifically, one specimen with a brittle intergranular fracture surface, one with a ductile transgranular fracture surface, and one with a fracture surface with both brittle intergranular and ductile transgranular areas are shown. In figure 3.5 one sees a series of pictures that was taken from a HCF specimen which should help to understand the logic behind the SEM analysis.

(a) Picture of specimen with normal camera

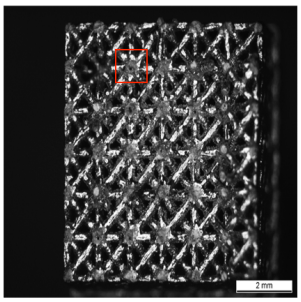

(b) Picture of bottom part of specimen under light microscope

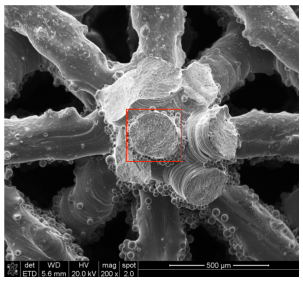

(c) Picture of node (row: 2, column: 3, see (b)); 200x magnification

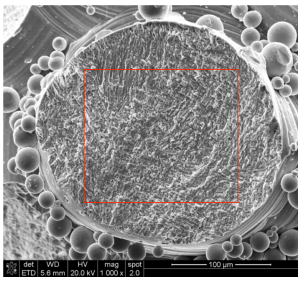

(d) Picture of central strut of node (see (c)), 1000x magnification

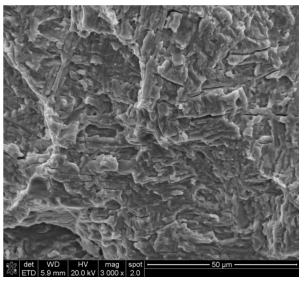

(e) Picture of the central strut (see (d)); 3000x magnification

Figure 3.5: Fractured lattice specimen tested in fatigue regime. $N = 577475$. Series of pictures from low (a) to high magnification (e). Red rectangles indicate which area is shown at higher magnification in next image.

3.4.2 Co-existence of different fracture types in fatigue specimens

The second observation made during the analysis of the fractured specimens under the SEM was the co-existence of different fracture types in the lattice specimens that were tested in fatigue regime. While the analysis of specimens that were tested in quasi-static regime revealed ductile transgranular fracture surfaces only, in the fatigue specimens all of the three different fracture types were observed. Additionally, it was found that the longer the fatigue life of a specimen, the more brittle intergranular surfaces that specimen contained. This is illustrated in figure 3.6.

3.4.3 Relation of angle of fracture surface and fracture type

In addition to the first two observations made during the microscopic analysis of the fracture surface, a relation of the angle of the fracture surface and the fracture type was found. More specifically, it could be seen that while in

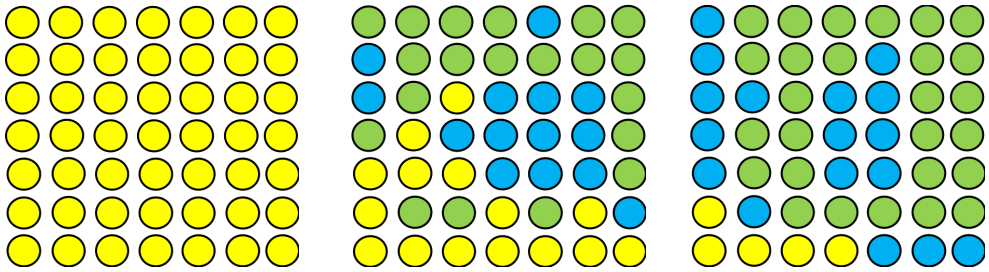

(a) Quasi-static specimen (b) LCF specimen, $N = 14385$ (c) HCF specimen, $N = 577475$

Figure 3.6: Co-existence of different fracture types. Yellow: ductile transgranular fracture, green: brittle intergranular fracture, blue: surface with both ductile transgranular and brittle intergranular fracture areas. (a) Quasi-static specimen (b) LCF specimen (c) HCF specimen

the quasi-static specimens both the quasi-perpendicular planes as well as the 45° planes always showed fracture of ductile transgranular type, in the HCF specimen both these planes revealed fractures of brittle intergranular type. The LCF specimens revealed a mixture, with brittle intergranular fracture being dominant in the quasi-perpendicular planes and ductile transgranular fractures dominating the 45° planes. This is illustrated in figure 3.7.

3.4.4 Analysis of struts

Microscopic analysis of the fracture surface of the strut specimens showed results that are consistent with those of the lattices.

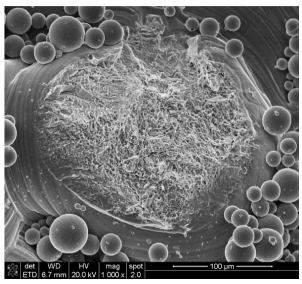

(a) Central strut of node, ductile transgranular fracture.

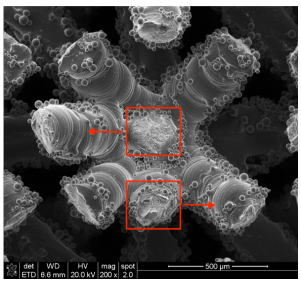

(b) Node of quasi-static specimen.

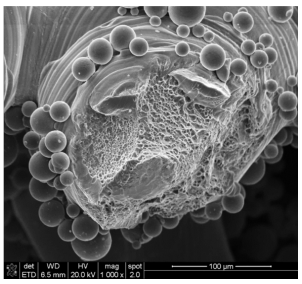

(c) Bottom strut of node, ductile transgranular fracture.

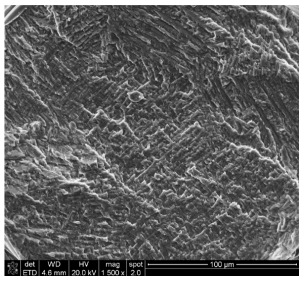

(d) Central strut of node, brittle intergranular fracture.

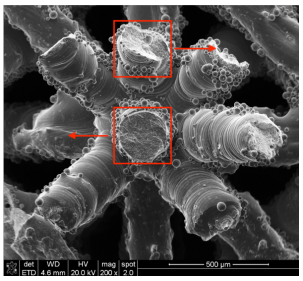

(e) Node of LCF specimen, $N = 14385$.

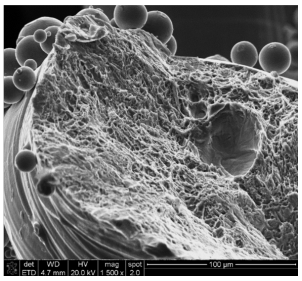

(f) Top strut of node, ductile transgranular fracture.

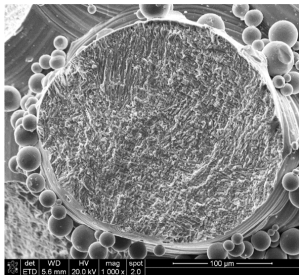

(g) Central strut of node, brittle intergranular fracture.

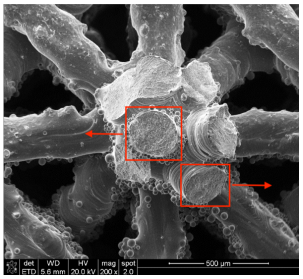

(h) Node of HCF specimen, $N = 577475$.

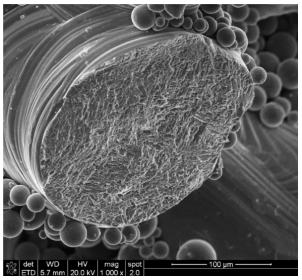

(i) Bottom right strut of node, brittle intergranular fracture.

Figure 3.7: Relation of angle of fracture surface and fracture type. Each row represent a different specimen. Row 1: quasi-static specimen. Row 2: LCF specimen, $N = 14385$. Row 3: HCF specimen, $N = 577475$. Red rectangles and arrows indicate which regions are show in higher magnification in the figures beside.

Chapter 4

Summary and Outlook

The objective of this research project was to investigate the fatigue behavior of AM Ti-6Al-4V lattices. In particular, their fatigue behavior should be predicted by the results of the analysis of single struts of the same material.

Experiments, microscopic analysis and finite element analysis have led to the following findings:

- Both AM Ti-6Al-4V struts and lattices performed worse in fatigue tests than bulk AM Ti-6Al-4V and than wrought Ti-6Al-4V.
- Lattices performed worse than struts.
- The manufacturing process of the specimens was inaccurate and led to substantial geometrical mismatches.
- Finite element analysis helped to determine realistic and effective cross-sectional areas for the lattice structures.
- Three different fracture types were observed. Ductile transgranular fracture mechanism was dominant in quasi-static specimens and brittle intergranular fracture mechanism was dominant in fatigue specimens.

In the future it would be interesting to investigate whether finite element analysis predicts failure at the same location as seen in the experiments. Moreover, additional fatigue test should be performed to increase reliability of the results. In addition, tests with a different stress ratio R should be performed, examining fully-reversed and compression-compression mode, to get a comprehensive understanding of the fatigue behavior of the lattice structures. Finally, it should be analyzed if the fracture surfaces of quasi-static specimens have a higher pore density than the fracture surfaces of fatigue specimens. Due to time reasons this was not followed up during the microscopic analysis.

Appendix A

Appendix

Element	Mass (%)
Titanium	Balance
Aluminium	5.50 to 6.50
Vanadium	3.50 to 4.50
Iron	≤ 0.25
Oxygen	≤ 0.13
Carbon	≤ 0.08
Nitrogen	≤ 0.05
Hydrogen	≤ 0.012
Yttrium	≤ 0.005
Residuals	≤ 0.10 each, ≤ 0.40 total

Figure A.1: Composition of Ti-6Al-4V powder as specified by the ASTM

	Heat treated (See note 2)		**HIP treated** (see note 6)	
	Mean	**Standard deviation (±1σ)**	**Mean**	**Standard deviation (±1σ)**
Ultimate tensile strength (UTS) (See note 3)				
Horizontal direction (XY)	1089 MPa	7 MPa	1033 MPa	4 MPa
Vertical direction (Z)	1085 MPa	12 MPa	1034 MPa	7 MPa
Yield strength (see note 3)				
Horizontal direction (XY)	1007 MPa	5 MPa	947 MPa	4 MPa
Vertical direction (Z)	985 MPa	23 MPa	923 MPa	21 MPa
Elongation at break (See note 3)				
Horizontal direction (XY)	16%	1%	16%	1%
Vertical direction (Z)	14%	1%	17%	1%
Modulus of elasticity (see note 3)				
Horizontal direction (XY)	129 GPa	7 GPa	127 GPa	3 GPa
Vertical direction (Z)	126 GPa	15 GPa	125 GPa	4 GPa
Hardness (Vickers) (see note 4)				
Horizontal direction (XY)	368 HV0.5	10 HV0.5	352 HV0.5	9 HV0.5
Vertical direction (Z)	372 HV0.5	7 HV0.5	360 HV0.5	7 HV0.5
Surface roughness (R_a) (See note 5)				
Horizontal direction (XY)	4 µm to 6 µm			
Vertical direction (Z)	4 µm to 7 µm			

Figure A.2: Mechanical properties of exemplary AM Ti-6Al-4V parts produced by Renishaw with a layer thickness of $30\mu m$

List of Figures

1.1 Hip Implant 2

2.1 Geometry of analyzed specimens 4
2.2 Test setup struts 5
2.3 Test setup lattices 6

3.1 Fatigue behavior of AM Ti-6Al-4V struts. 9
3.2 Fatigue behavior of AM Ti-6Al-4V lattices. 11
3.3 Finite element analysis 11
3.4 Three different fracture types 12
3.5 Series of SEM pictures of HCF specimen 13
3.6 Co-existence of different fracture types 14
3.7 Relation of angle of fracture surface and fracture type 15

A.1 Ti-6Al-4V powder composition 19
A.2 Mechanical properties of AM Ti-6Al-4V components 19

List of Tables

2.1 Stress / force levels used in MFL tests 4
2.2 Parameters of FE model 6

3.1 Results of staircase test data, struts 10
3.2 Results of staircase test data, lattices 10

Bibliography

[1] K. V. Wong and A. Hernandez, "A review of additive manufacturing," *ISRN Mechanical Engineering*, vol. 2012, 08 2012.

[2] M. Mani, K. W. Lyons, and S. K. Gupta, "Sustainability characterization for additive manufacturing," *Journal of research of the National Institute of Standards and Technology*, vol. 119, pp. 419–428, 09 2014.

[3] U. E. Klotz, D. Tiberto, and F. Held, "Additive manufacturing of 18-karat yellow-gold alloys," in *Santa Fe Symposium on Jewelry Manufacturing Technology*, 05 2016, pp. 255–272.

[4] J. Kranz, D. Herzog, and C. Emmelmann, "Design guidelines for laser additive manufacturing of lightweight structures in Ti-6Al-4V," *Journal of Laser Applications*, vol. 27, no. S1, 02 2015.

[5] Y. He, D. Burkhalter, D. Durocher, and J. M. Gilbert, "Solid-lattice hip prosthesis design: Applying topology and lattice optimization to reduce stress shielding from hip implants," 04 2018.

[6] G. Chahine, M. Koike, T. Okabe, P. Smith, and R. Kovacevic, "The design and production of Ti-6Al-4V eli customized dental implants," *Jom*, vol. 60, no. 11, pp. 50–55, 11 2008.

[7] P. Li, D. Warner, A. Fatemi, and N. Phan, "Critical assessment of the fatigue performance of additively manufactured Ti-6Al-4V and perspective for future research," *International Journal of Fatigue*, vol. 85, 12 2015.

[8] J. Majumdar and I. Manna, "Introduction to laser assisted fabrication of materials," *Laser-Assisted Fabrication of Materials, Springer Series in Materials Science, Volume 161. ISBN 978-3-642-28358-1. Springer-Verlag Berlin Heidelberg, 2013, p. 1*, 11 2013.

[9] J.-P. Kruth, G. Levy, F. Klocke, and T. Childs, "Consolidation phenomena in laser and powder-bed based layered manufacturing," *CIRP Annals*, vol. 56, no. 2, pp. 730–759, 01 2007.

[10] Y. He, "Applying topology and lattice optimization to reduce stress shielding from hip implants," 05 2018, date of access: 2019-05-28.

[11] "Metallic materials – Fatigue testing – Statistical planning and analysis of data," International Organization for Standardization, Geneva, CH, Standard, 03 2003.

Eidgenössische Technische Hochschule Zürich
Swiss Federal Institute of Technology Zurich

Declaration of originality

The signed declaration of originality is a component of every semester paper, Bachelor's thesis, Master's thesis and any other degree paper undertaken during the course of studies, including the respective electronic versions.

Lecturers may also require a declaration of originality for other written papers compiled for their courses.

I hereby confirm that I am the sole author of the written work here enclosed and that I have compiled it in my own words. Parts excepted are corrections of form and content by the supervisor.

Title of work (in block letters):

Authored by (in block letters):
For papers written by groups the names of all authors are required.

Name(s):	**First name(s):**

With my signature I confirm that

- I have committed none of the forms of plagiarism described in the 'Citation etiquette' information sheet.
- I have documented all methods, data and processes truthfully.
- I have not manipulated any data.
- I have mentioned all persons who were significant facilitators of the work.

I am aware that the work may be screened electronically for plagiarism.

Place, date	**Signature(s)**

For papers written by groups the names of all authors are required. Their signatures collectively guarantee the entire content of the written paper.